Flow Separation at the Upper Domes with Various Rayleigh Numbers and Truncation Angles

Su-Yeon Park and Bum-Jin Chung
Department of Nuclear Engineering, Kyung Hee University
#1732 Deogyeong-daero, Giheung-gu, Yongin-si, Gyeonggi-do, 17104, Korea
Corresponding author: bjchung@khu.ac.kr

***Keywords : Small Modular Reactors, Natural convection, Dome, Flow separation**

1. Introduction

The concept of passive cooling, has become an essential design feature in small modular reactors (SMRs), which maintains core integrity through natural driving forces without external driving force or human intervention. In addition, due to their smaller size compared to conventional nuclear power plants (NPPs), SMRs utilize the steel containment vessel (CV) more extensively as a passive cooling system. During a severe accident, the evaporated coolant released from the reactor vessel, rises and transfers heat to the upper region of the containment vessel. The upper dome can condense this vapor through external natural convection cooling, thereby reducing the internal pressure of the CV [1-3].

Although SMRs are smaller than conventional NPPs, they fall within the high Rayleigh number (Ra_{Db}) regime in terms of natural convection scale. In licensed or currently designed SMRs (e.g., VOYGR, i-SMR, and ACP100), the Ra_{Db} of the upper dome exceeds 10^9 [4]. Furthermore, natural convection over the dome varies depending on its geometric characteristics, particularly the truncation angle, which is defined as the angle from the leading edge to the apex of the dome, as described in Fig. 1. The truncation angle of SMRs ranges from 40° to 90°.

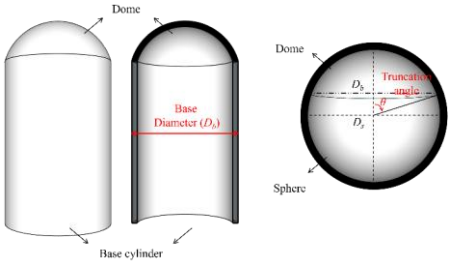

Fig. 1. Schematic image of dome characteristic factors; base diameter (D_b) and truncation angle (θ).

In the upward dome-structure, the flow separation occurs due to the direction difference between buoyancy force and heated surface. In the stable flow region, the local heat transfer decreases as the thermal boundary layer becomes thicker. However, the wake formed by flow separation brought fresh fluid to the surface and local heat transfer increased [5-7]. Therefore, as the Ra_{Db} increases, the flow separation point moves upstream location and the resulting increase in heat transfer significantly affects the total heat transfer of the dome. The Ra at which the effect of flow separation begins to significantly influence the average heat transfer is defined as the critical Ra.

Kitamura and Kimura [8] studied natural convection flow and heat transfer over a horizontal disk, which is equivalent to a dome with θ = 0°. They proposed a Ra criterion for the flow separation point. The radial distance from the leading edge to the separation point was adopted as the characteristic length, denoted by r_s. Ra_{rs} is identical for a given Pr, even when the disk diameter or ΔT varied. Fig. 2 shows the Ra_{rs} of the disk for Pr = 0.7 and Pr = 7. The coefficients of variation were 19.5 and 24.4, respectively.

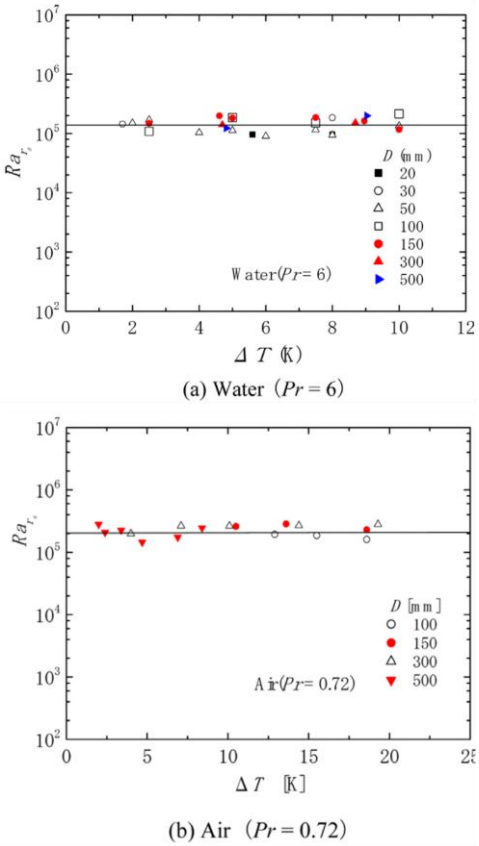

Fig. 2. Ra_{rs} of disk with various diameter (D) and ΔT [2].

If the separation point can be tracked, a more refined design of upper dome cooling becomes possible. However, to achieve this, further studies are required to evaluate the applicability and relationships of the model for domes with a wider range of θ and under various Pr conditions. Therefore, this study aims to establish the separation prediction model for a wider range of θ and to investigate the effect of the Pr.

2. Experimental method

2.1 Mass transfer method

In this experiment, heat transfer experiments will be substituted with mass transfer experiments using the analogy concept [9]. The governing equations for heat and mass transfer are analogous and belong to the same mathematical class. In heat transfer system, temperature (T) and thermal diffusivity (α) can be directly compared to concentration (C) and mass diffusivity (D_m) in mass transfer systems. In this study, a $CuSO_4$-H_2SO_4 copper electroplating system was chosen. When an electric potential is applied to electrodes submerged in a $CuSO_4$-H_2SO_4 aqueous solution and are subsequently reduced at the cathode. The concentration between the cathode surface and the bulk fluid is analogous to the temperature difference between the heater surface and the bulk fluid, while the current density represents the heat flux. However, accurately measuring the concentration of cupric ions at the cathode surface during mass transfer experiments is challenging, so the limit current technique is employed [10].

This experimental technique, based on the heat and mass transfer analogy, has been employed by various researchers [11, 12]. Typically, D_m is much smaller than α, making mass transfer systems particularly suitable for simulating fluids with high Prandtl numbers (Pr). This system is effective in achieving high Ra_{Db}. Table 1 presents the corresponding governing parameters for both heat and mass transfer systems. The mass transfer coefficient (h_m) can be obtained by Eq. (1).

$$h_m = \frac{(1-t_n)I_{\lim}}{nFC_b} \tag{1}$$

Table 1. Dimensionless numbers for the analogous systems.

Heat transfer		Mass transfer	
Nu	h_hD/k	Sh	h_mD/D_m
Pr	ν/α	Sc	ν/D_m
Ra_{Db}	$g\beta\Delta TD_b^3/\alpha\nu$	Ra_{Db}	$GD_b^3/D_m\nu$

2.2 Test matrix and rig

Table II presents the test matrix, and the Pr was fixed at 2094. For the dome with a truncation angle of 90°, three experimental cases with different D_b values were conducted under otherwise identical conditions to compare Ra_{rs}. For domes with θ other than 90°, only one case was performed for each angle, and only Ra_{rs} was measured.

Table 2. Test matrix.

Pr	D_b (m)	Ra_{Db}	θ (°)
2094	0.04	1.08×10^{10}	30, 90
	0.1	1.68×10^{11}	90
	0.2	1.35×10^{12}	70
	0.4	1.08×10^{13}	90

Figure 3 shows the experimental apparatus of $\theta = 70°$ dome with $Ra_{Db} = 1.35 \times 10^{12}$ and it's arrangement in the tank. To effectively simulate the curved surface of the dome, the cathode was fabricated by attaching copper foil to a 3D-printed structure. To observe the local h_m, piecewise electrodes densely arranged in the circumferential direction were employed. The electrodes were configured more densely near the leading edge, where flow separation was expected, than near the apex.

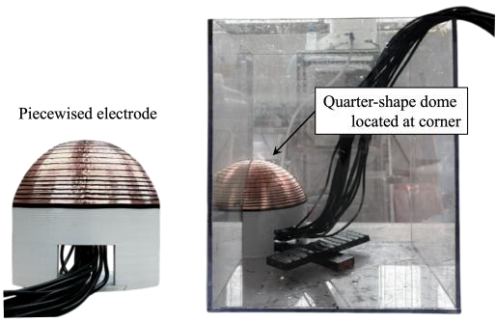

Fig. 3. Experimental apparatus: piecewise cathode for the $\theta = 70°$ dome with $Ra_{Db} = 1.35 \times 10^{12}$.

Figure 4 shows the schematic image of the experimental apparatus along with its electrical circuit diagram. The quarter-shape dome was positioned at the corner of the tank, and the electric wires connected to the copper foil were routed inside the dome and connected to the NI device outside the tank through a passage in the lower support structure. The anodes were located on the tank wall surrounding the cathode assembly. Power was supplied through a power source (Vüpower K1810), and current was measured and recorded using a DAQ (NI9227).

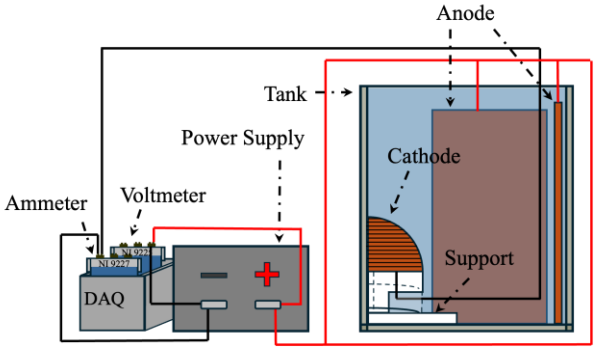

Fig. 4. Diagram of the experimental apparatus with electrical circuit diagram.

3. Results and discussion

3.1 Application of the Ra_{rs} to natural convection over a sphere

In our experiment, *Sc*, which is analogous to the *Pr* in heat transfer, was fixed; therefore, the applicability of Ra_{rs} with respect to *Pr* could not be confirmed. To address this limitation, we collected available separation point data from the literature and calculated the corresponding Ra_{rs} values. The most accessible data in previous studies were obtained for spherical geometries.

For a sphere, r_s was defined as the radial distance from the edge of the equatorial cross-section to the perpendicular projection of the separation point. Fig. 5 illustrates the schematic definition of r_s for a sphere.

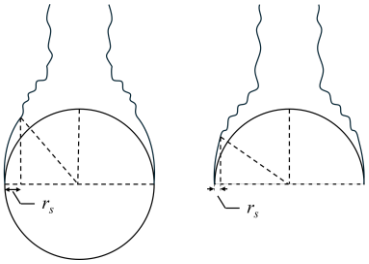

Fig. 5. Schematic image of r_s for sphere and hemisphere.

Kitamura et al. (2015) [13] measured the flow separation at $Pr = 6$ through the flow visualization in a heat transfer experiment, while Lee et al. (2017) [14] measured the flow separation at $Pr = 2094$ by observing the minimum local h_m in a mass transfer experiment. Fig. 6 shows a plot of the calculated Ra_{rs} based on the separation points measured by the two studies. The average Ra_{rs} for a sphere at $Pr = 6$ is 2.6×10^7, with a coefficient of variation is 21.7. For $Pr = 2094$, the average Ra_{rs} is 7.1×10^7, with a coefficient of variation of 17.7. The concept of Ra_{rs} was found to be valid for the spherical geometry.

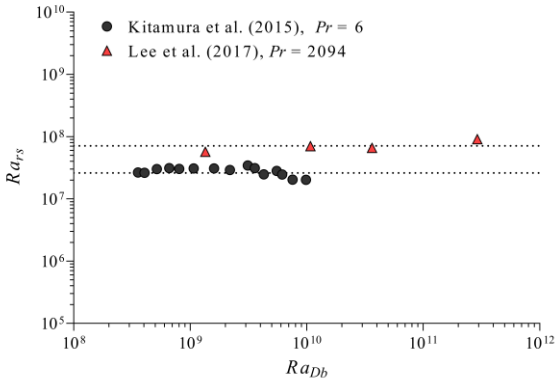

Fig. 6. Ra_{rs} calculated using the sphere separation point data at $Pr = 6$ and $Pr = 2094$ reported in the existing study [13, 14].

3.2 Ra_{rs} over a dome with various θ

Figure 7 shows the measured local h_m for the $\theta = 90°$ dome at $Ra_{Db} = 1.08 \times 10^{10}$, 1.68×10^{11}, and 1.08×10^{13}. The *x*-axis represents the polar angle from the leading edge, denoted as φ, where $\varphi = 0°$ at the leading edge and $\varphi = 90°$ at the apex.

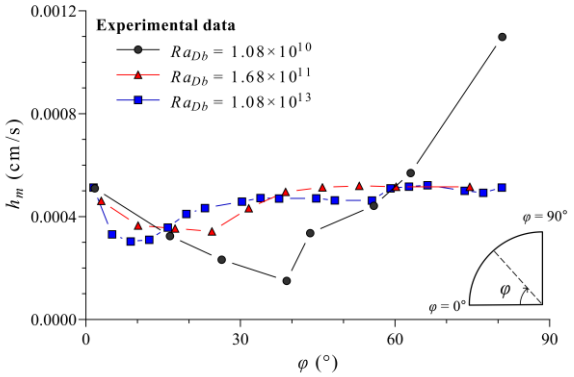

Fig. 7. Local h_m according to the polar angle (φ).

The local h_m decreases near the leading edge as the boundary layer thickens and increases after flow separation. For the dome at $Ra_{Db} = 1.08 \times 10^{10}$, the local h_m increases continuously up to the apex. In contrast, for the domes at $Ra_{Db} = 1.68 \times 10^{11}$ and 1.08×10^{13}, it increases initially and then levels off. This occurs because flow separation develops further upstream than plume development, leading to earlier detachment and preventing mixing with fresh fluid by the outer layer flows that form the plume.

For all cases, the location where the local h_m reached its minimum value was identified as the separation point. Using the measured separation point, the radial distance r_s was calculated in the same manner as for a sphere; namely, from the leading edge of the base surface to the point obtained by dropping a perpendicular line from the separation point onto the base surface. Fig. 8 shows the Ra_{rs} of $\theta = 90°$ dome. At $Pr = 2094$, the mean Ra_{rs} value for the $\theta = 90°$ dome is 1.47×10^7, with a coefficient of variation of 3.3%.

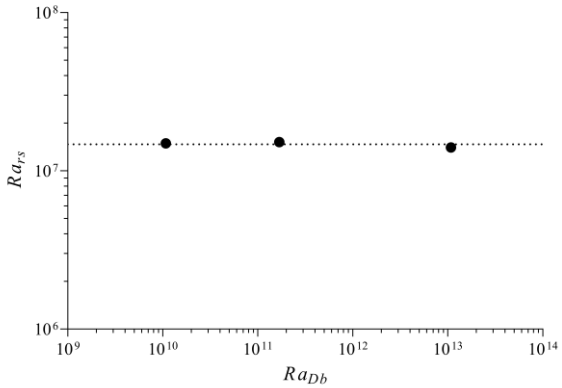

Fig. 8. Ra_{rs} for $\theta = 90°$ dome with different D_b.

The validity of the Ra_{rs} analysis was confirmed for the sphere, the $\theta = 0°$ dome, and the $\theta = 90°$ dome. For the $\theta = 70°$ and $\theta = 30°$ domes, Ra_{rs} was likewise determined at a given Ra_{Db} using the same methodology applied to the $\theta = 90°$ dome. Fig. 9 presents the measured distribution of the local h_m. Based on the separation points identified from these results, the calculated Ra_{rs} values are 4.39×10^7 for the $\theta = 70°$ dome and 7.59×10^6 for the $\theta = 30°$ dome.

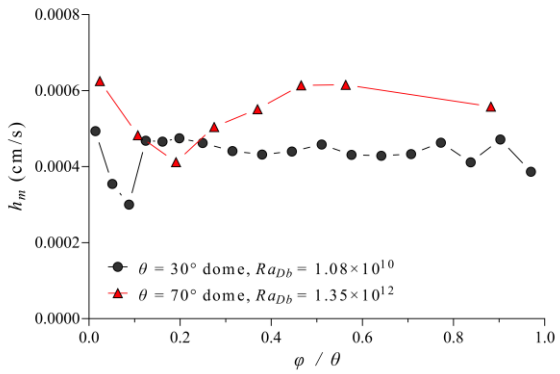

Fig. 9. Local h_m according to the polar angle ratio.

Figure 10 shows the variation of Ra_{rs} with dome truncation angle at $Pr = 2094$. It is observed that as the truncation angle of the dome decreases, flow separation occurs earlier, leading to a reduction in Ra_{rs}. This is because the instability arising from the misalignment between the buoyancy force and the surface orientation becomes more pronounced as the θ of the dome decreases. Furthermore, this result is consistent with previous study [4] reporting that the average Nu_{Db} of the dome decreases as the θ becomes smaller.

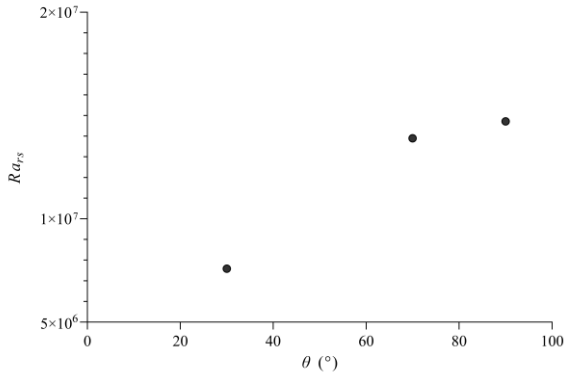

Fig. 9. Ra_{rs} for dome according to the truncation angle.

4. Conclusions

In this study, the criterion for the separation point defined for a horizontal disk (i.e., a dome with a truncation angle of 0°) was experimentally extended to domes with different truncation angles. When Ra_{rs} was calculated using the separation point data for a sphere reported in the literature, it was observed to remain constant over a wide range of Ra_D. The value of Ra_{rs} varied depending on Pr. For high Pr ($Pr = 2094$), Ra_{rs} was 7.1×10^7, which is larger than 2.6×10^7 for low Pr ($Pr = 6$).

When Ra_{rs} was measured for a 90° truncation-angle dome at $Pr = 2094$, it was determined to be 1.4×10^7 with a very small coefficient of variation. For a 30° truncation angle dome at $Ra_{Db} = 1.08 \times 10^{10}$ and a 70° truncation angle dome at $Ra_{Db} = 1.35 \times 10^{12}$, the measured Ra_{rs} decreased as the truncation angle decreased. This indicates that, for smaller truncation angles, flow separation develops earlier, which is consistent with the observed trend that the average heat transfer of the dome decreases as the truncation angle decreases. Accordingly, follow-up studies will be conducted to investigate the effect of the Pr, so that the experimentally confirmed Ra_{rs} values for various domes can be extended to a wider range of Pr.

5. Acknowledgements

This work was supported by the Innovative Small Modular Reactor Development Agency grant funded by Korea Government Ministry of Climate, Energy and Environment (MCEE) (No. RS-2024-00404240).

REFERENCES

[1] C. Dong, S. Chen, R. Chen, W. Tian, S. Qiu, G.H. Su, Numerical simulation of natural convection around the dome in the passive containment air-cooling system, Nuclear Engineering and Technology, Vol. 55(8), p. 2997-3009, 2023.
[2] J. Liu, F. Niu, B. Ahmad, Z. Guo, H. Zhu, Z.a. Tan, G. Jin, Flow characteristics in the containment cooling pools of small modular reactors, International Journal of Heat and Mass Transfer, Vol. 133, p. 445-460, 2019.
[3] J. Zhang, J. Liu, W. Lu, Study on Laminar Natural Convection Heat Transfer from a Hemisphere with Uniform Heat Flux Surface, Journal of Thermal Science, Vol. 28(2), p. 232-245, 2018.
[4] S.-Y. Park, D.-H. Park, B.-J. Chung, Natural convection experiments around an upper dome varying Rayleigh number and truncation angle, Experimental Thermal and Fluid Science, Vol. 169, p. 111548, 2025.
[5] S. Mori, A. Tanimoto, M. Yamashita, M. Aoki, K. Yasuda, Mass transfer by laminar free convection from a solid sphere, Kagaku Kogaku Ronbunshu, Vol. 2(2), p. 214-216, 1976.
[6] G. Schütz, Natural convection mass-transfer measurements on spheres and horizontal cylinders by an electrochemical method, International Journal of Heat and Mass Transfer, Vol. 6(10), p. 873-879, 1963.
[7] A.A. Kranse, J. Schenk, Thermal free convection from a solid sphere, Applied Scientific Research, Section A, Vol. 15(1), p. 397-403, 1966.
[8] K. Kitamura, F. Kimura, Fluid flow and heat transfer of natural convection over upward-facing, horizontal heated circular disks, Heat Transfer—Asian Research, Vol. 37(6), p. 339-351, 2008.
[9] A. Bejan, Mass Transfer, in: Convection Heat Transfer, p. 489-536, 2013.
[10] S.-H. Ko, D.-W. Moon, B.-J. Chung, Applications of electroplating method for heat transfer studies using analogy concept, Nuclear engineering and Technology, Vol. 38(3), p. 251-258, 2006.
[11] D.W. Hubbard, E.N. Lightfoot, Correlation of Heat and Mass Transfer Data for High Schmidt and Reynolds Numbers,

Industrial & Engineering Chemistry Fundamentals, Vol. 5(3), p. 370-379, 1966.
[12] F.P. Berger, K.F.F.L. Hau, Mass transfer in turbulent pipe flow measured by the electrochemical method, International Journal of Heat and Mass Transfer, Vol. 20(11), p. 1185-1194, 1977.
[13] K. Kitamura, A. Mitsuishi, T. Suzuki, T. Misumi, Fluid flow and heat transfer of high-Rayleigh-number natural convection around heated spheres, International Journal of Heat and Mass Transfer, Vol. 86, p. 149-157, 2015.
[14] D.-Y. Lee, B.-J. Chung, Visualization of natural convection heat transfer on a sphere, Heat and Mass Transfer, Vol. 53(12), p. 3613-3620, 2017.